Proceedings of the ASME 2022
International Design Engineering Technical Conferences and
Computers and Information in Engineering Conference
IDETC/CIE2022
August 14-17, 2022, St. Louis, Missouri
DOI: 10.1115/DETC2022-91006

DETC2022-91006

MECHANICAL FACE SEAL DYNAMICS SUBJECTED TO MACHINE VIBRATION AND NOISE

Itzhak Green (Fellow, ASME)
green@gatech.edu
Woodruff School of Mechanical Engineering, Georgia Institute of Technology, Atlanta, GA

ABSTRACT

Mechanical face seals are wide-spread in many applications, such as centrifugal compressors, submersible pumps, drill-bits for oil and water, hydrocarbon processing equipment, and turbomachinery. Often vibration and noise are unavoidable because of changing environments which can be persistent and forceful. In critical applications when seals fail, they may have significant or even catastrophic consequences. To ensure the safety of such machinery and its associated mechanical components, the vibration and noise must be diagnosed and kept within certain limits. This work focuses on the dynamics of a flexibly mounted stator mechanical face seal that is subjected to combinations of axial broad-band noisy vibrations of the shaft and the housing. The current analysis builds upon the dynamic models that have been developed over the last four decades. In all that body of work, the positions of the housing and the shaft have been considered fixed. The current work relaxes that condition, augmenting the equations of motion to incorporate the said noisy vibrations. While the exact root-causes and sources of machinery vibration are very difficult to ascertain, the current analysis uses some general common causes of noisy seal operation, and provides markers to be observed for diagnosis. While the forcing noises are assumed to originate along the main axis of the seal, because of the strong coupling between the axial and angular modes, the seal is affected (even strongly) in all modes (axial and angular). A numerical simulation ensues, and the results are subject to spectral analyses. Results show that under some design conditions, the seal is largely insensitive to machine vibrations. However, under other design parameters, the seal response exhibits a rich spectral content that stems from various transient phenomena that include (among others) half frequency whirl, synchronous steady-state response, and the natural (eigen) response. Under aggravated noisy conditions the investigated seal exhibits large oscillations and leakage, along with face contact and rubbing. Prolonged rubbing causes faces to wear and leads ultimately to seal failure.

Keywords: Mechanical Face Seals, Dynamics, Machine Noise and Vibration, Frequency Response, Rubbing Contact.

NOMENCLATURE

B	=	balance ratio, Table 1
C	=	centerline varying clearance, C_o+Z
C_o	=	design clearance, Table 1
D_{Zs}	=	support axial damping coefficient, Table 1
F	=	force, Table 1
h	=	local film thickness, Table 1
I	=	transverse moment of inertia
K_{Zs}	=	support axial stiffness coefficient, Table 1
M	=	moment
m	=	stator mass, Table 1
p	=	pressure
Q	=	flow
r	=	radial coordinate, Table 1, Fig. 1
t	=	time
Z	=	stator absolute axial degree of freedom, Fig. 1
Z_h	=	axial housing vibration, Fig. 1
Z_r	=	axial rotor (shaft) vibration, Fig. 1
β	=	face coning, Table 1
γ	=	relative misalignment, $\vec{\gamma} = \vec{\gamma}_s - \vec{\gamma}_r$
γ_o	=	relative misalignment caused by rotor runout alone
γ_r	=	rotor runout, Table 1, Fig. 1
γ_s	=	stator nutation, Fig. 1
γ_{si}	=	stator initial misalignment
γ_{sI}	=	steady-state stator response due to γ_{si} alone
γ_{sr}	=	steady-state stator response due to γ_r alone
θ	=	angular coordinate
μ	=	viscosity, Table 1
τ	=	thermal time constant, Table 1
ψ	=	precession
ω	=	shaft angular velocity at steady-state, Table 1

Subscripts

c	=	contact
i	=	inner radius
min	=	minimum film thickness
o	=	outer radius
r	=	rotor
ref	=	reference value
s	=	stator, or flexible support

1. INTRODUCTION

Mechanical face seals are complex systems, where dynamics, fluid film hydrodynamics, and thermoelastic effects are present and coupled to each other. A successful seal design must be tolerant of all these effects to co-exist. Over the last four decades successful models have incorporated such effects singularly or collectively, including transient operations, but invariably they have all considered the surrounding to be pristine. Frequently, however, machines in which seals operate are subject to autonomous vibration. The seals inevitably respond to such vibration in manners that can be quite substantial and perhaps even destructive.

Very few previous works consider equipment noise and vibrations as they affect seals. Durham et al. [1] provide data from field installations of electric submersible pumps. They conclude that equipment vibration is inherent in seal design, manufacture, and application. A large percentage of pump failures may be attributed to seals that are unable to withstand high vibration, ultimately leading to motor and pump failures. Kim et al. [2] experimentally study the squeal noise and vibration of a mechanical seal used in an automotive water pump. The frequency spectra of both noise and vibration signals are obtained for various speeds of the pump, and waterfall plots for noise and vibration are constructed showing a relation between the natural frequencies, excitation frequencies, and squeal noise frequencies. Stefanko and Leishear [3] experimentally show that a reduction of radial vibrations in mechanical seals increases the life of the seals in centrifugal pumps. Many testimonies, gathered from end-users and seals' original equipment manufacturers, describe the dire consequences that machine vibration have upon seals' survivability. Most of these testimonies are hearsay of personal experiences; nevertheless, these effects do exist and must be understood.

The objective here is, therefore, to extend computational means to investigate the transient dynamic behavior of mechanical face seals subject to machine vibration. The analysis herein augments comprehensive models that have already been developed [4–37]. The said models included angular and axial modes of dynamic response in transient and steady-state operations [29,31,35,38], face transient warping, i.e., time-varying coning incorporated via transient thermoelastic deformation [39,40], and rough surface elastoplastic contact of the seal faces [36]. All these effects had been coupled in a comprehensive model that simulates start-up to shut-down transient operation [41]. The theoretical models [4–9,11–14,19,20,23,24,26–31,33–38,41] have been verified through extensive experimentation [10,15,17,18,21,22,25,26,28,32,42]. These theoretical models provide the foundation for the current analysis. While in all of the previous analyses the seal enclosure is assumed to be inertial, here, that condition is relaxed. The current study expands the theoretical models, the computational means, and the diagnostics markers that are typical in the dynamics of flexibly-mounted stator (FMS) mechanical face seals, affected by broad-spectrum machine vibration. Because an analytical closed-form solution that accounts for all of the effects is patently not feasible, the investigation herein offers a comprehensive non-linear numerical simulation for the transient response of a face seal that is subjected to its own forcing misalignments, and now as well, machine vibration. The non-linear nature of the problem is due to face (asperity) contact, cavitation, and large axial and angular excursions. Results are provided for the most important seal performance outcomes, such as the axial seal face excursion, the relative tilt between the stator and the rotor, the minimum film thickness, and the leakage.

2. MODEL FOR ANALYSIS

This work fully builds upon all of the aforementioned analyses, with [41] being the foundation, and, hence, the modeling sections on face deformation caused by mechanical and thermal effects, the kinematics, and the method of solution remain intact (see details in [41]). Only the main changes made to the said work are highlighted herein. The changes stem from the noises imparted by the rotor and housing mechanical vibrations.

Figure 1 shows the schematics of a mechanical seal. Parameters are described in the Nomenclature and in [41]. The stator is the flexibly-mounted (floating) face, and the rotor is a face fixed to the rotating shaft. A kinematical model is shown in Fig. 2, where a detailed model description is given in [5–7,29,35,41], and that remains intact. Of importance here are the stator response to its own initial misalignment and rotor runout:

$$\vec{\gamma}_s = \vec{\gamma}_{sI} + \vec{\gamma}_{sr} \quad (1)$$

The relative tilt between the faces is measured between the total stator response in Eq. (1), and the rotor runout:

$$\vec{\gamma} = \vec{\gamma}_s - \vec{\gamma}_r ;\ |\gamma| = \left[\gamma_s^2 + \gamma_r^2 - 2\gamma_s\gamma_r\cos(\psi - \psi_r)\right]^{1/2} \quad @ \quad \psi_r(t) = \int_0^t \dot{\psi}_r dt \quad (2)$$

The seal clearance at the sealing dam is typically of the order of a micron in modern applications. This is where asperity contact and face deformation take place. Seal leakage and wear (survivability) are two competing design objectives that are strongly influenced by asperity contact, and face deformation.

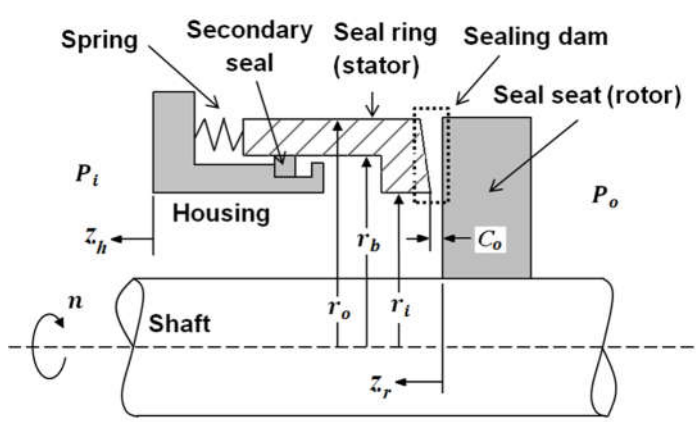

Fig. 1 Mechanical face seal schematics showing rotor and housing random excitations (noises), Z_h, and, Z_r, respectively

2.1 Asperity Contact and Thermo-Elastic Deformation

The asperity contact model in [41] is based upon an outdated Chang et al. (CEB) model [43]. That model is replaced here by the Jackson-Green (JG) model [44] being the most robust and accurate to date. More details are given in the latter work, where the statistical accumulation of all asperity effects is done according to [45]. An off-line curve fit is used for expediency [36] expressing the local (nodal) contact pressure versus fluid film thickness. Ultimately, this process results in:

$$p_c(r,\theta,t) = C_1 \exp\left[C_2 h(r,\theta,t)\right] \tag{3}$$

Where C_1 and C_2 are fit parameters specific to surfaces roughness and seal face materials (given in Table 1).

Seal face coning, $\beta=\beta(t)$, is generated by time-dependent thermo-elastic deformation. The coning is schematically shown in Fig. 1 by the tapered sealing dam. Shaft rotation distributes the heat generation equally across the seal surface, allowing the thermo-elastic deformations to be governed by a first-order model [41]:

$$\tau\dot{\beta} + \beta = \beta_{ref}\left[\left(\frac{h_{ref}}{\bar{h}}\right)\left(\frac{\omega_r}{\omega_{ref}}\right)^2 + \frac{Q_f}{(Q_v)_{ref}}\right] \tag{4}$$

where τ is a thermal time constant. The first term on the right hand side is caused by the viscous heat generation, while the second term originates from traction being the result of a friction coefficient, f, and the contact pressure, p_c. Both heat generation mechanisms are given by:

$$\begin{aligned} Q_f &= \int_0^{2\pi}\int_{r_i}^{r_o} f\, p_c(r,\theta)\omega_r r^2 dr d\theta \\ (Q_v)_{ref} &= \int_0^{2\pi}\int_{r_i}^{r_o} \frac{\mu\omega_{ref}^2}{h_{ref}} r^3 dr d\theta \end{aligned} \tag{5}$$

The reference coning, β_{ref}, is obtained from an off-line finite element analysis of heat transfer of the entire seal structure. Commonly, Q_f is orders of magnitudes smaller than $(Q_v)_{ref}$, and typically it can be neglected.

2.2 Noise Excitation

This section contains the main kinematical changes viz-å-viz the model in [41] as caused by rotor and housing random vibrations. These noises impose additional forcing mechanisms in the equations of motion, which now need modifications.

Two forcing excitations are shown in Fig. 1. The machine (i.e., housing) may have a random axial vibration, Z_h, along with an axial random vibration of the shaft (i.e., rotor), Z_r, where both may occur synchronously or asynchronously. The former applies when the shaft is riding on bearings attached to the housing, which is the case considered here. A kinematical model is shown in Fig. 2, where a detailed model description is given in [5,7,29,41], and that remains intact. While Z_r affects directly the film thickness, Z_h forces the stator axially via the circumferential springs. Only one of the many circumferential springs supporting the stator (see Fig.1) is shown in Fig. 2, but effectively it represents all springs.

In addition to the said two axial noises, the shaft, due to its flexibility, might force a noisy (time-varying) runout:

$$\vec{\gamma}_r = \left[\gamma_r + \delta w(t)\right]\hat{\gamma}_r \tag{6}$$

Where $\delta w(t)$ is a white noise shaft misalignment. In the current model the said vibrations are assumed to take place mainly in the axial mode; however, because of the physical coupling with the angular modes, all modes experience noisy operation just as well. Hence, for simplicity it is assumed that $\delta w(t)=0$.

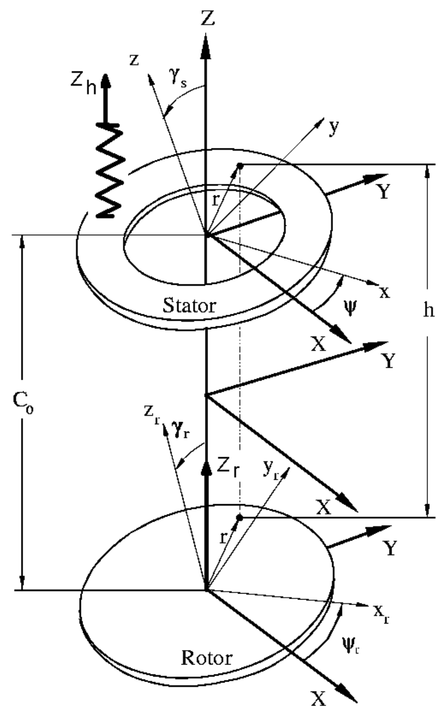

Fig. 2 A kinematical model showing excitations Z_h and Z_r

2.2 Noise Signals Modeling

The noises, Z_h and Z_r, can be simulated in various ways: (1) a white noise using a random number generator, (2) a time series (summation) of harmonics having random amplitudes, phases, and frequencies within respective frequency ranges of interest, and (3) a Weierstrass-Mandelbrot (WM) fractal function along with its derivatives [46]. The latter can be deterministic (default) or random (when random phases are added). Hence, Z_h and Z_r along with their time derivatives are available in the forgoing. The noise maximum magnitude is *4%* of the seal clearance, C_o.

2.3 Housing and Rotor Vibration Effects

The film thickness is [5,7,29,41]:

$$h(r,\theta,t) = C_o + \left[Z(t) - Z_r(t)\right] + \gamma(t) r\cos(\theta) + \beta(t)\left(r - r_i\right) \tag{7}$$

Which is needed for the solution of the Reynolds equation for incompressible fluids [7,41]:

$$\vec{\nabla}\cdot\left[\frac{h^3\vec{\nabla}p}{12\mu} - \frac{1}{2}\omega r h\,\vec{i}_\theta\right] = \frac{\partial h}{\partial t} \tag{8}$$

which is subject to boundary and initial conditions of the unknown pressure, $p=p_f(r,\theta,t)$. Clearly p depends upon h, and via $\partial h/\partial t$ it depends also upon $\dot{Z}_r$ by way of Eq. (7). The solution of Eq. (8) for $p=p_f(r,\theta,t)$ is presented in closed-form by Green and Etsion [5,7] and it is not repeated. Pressures from asperity contact, p_c, calculated by Eq. (3), and the fluid film pressures, $p_f(r,\theta,t)$, are added together, and integrated over the sealing dam area to yield film total opening moments and force:

$$\begin{aligned} M_{fx} &= \int_0^{2\pi}\int_{r_i}^{r_o}\left(p_f(r,\theta,t)+p_c(r,\theta,t)\right)r^2\sin\theta\, dr\, d\theta \\ M_{fy} &= -\int_0^{2\pi}\int_{r_i}^{r_o}\left(p_f(r,\theta,t)+p_c(r,\theta,t)\right)r^2\cos\theta\, dr\, d\theta \\ F_{fz} &= \int_0^{2\pi}\int_{r_i}^{r_o}\left(p_f(r,\theta,t)+p_c(r,\theta,t)\right)r\, dr\, d\theta \end{aligned} \quad (9)$$

The applied moment and force acting upon the stator are given by Eqs. (21) in [41], where the only changes needed are in the axial force containing the housing and shaft vibrations:

$$\begin{aligned} M_{sx} &= -K_s(\gamma_s-\gamma_{si}\cos\psi)-D_s\dot{\gamma}_s \\ M_{sy} &= -K_s\gamma_{si}\sin\psi-D_s\dot{\psi}\gamma_s \\ F_{sZ} &= -K_{Zs}(Z-Z_h)-D_{Zs}(\dot{Z}-\dot{Z}_h) \end{aligned} \quad (10)$$

Note that K_s and D_s are the support angular stiffness and damping, while K_{Zs} and D_{Zs} are their corresponding axial counterparts. These are either obtained from experimentation [42] or estimated from FEA [12,13].

2.4 Numerical integration in time of the EOM

The equations of motion (EOM) and the time-dependent coning (of Eq. (4)) are cast in a state-space form, as given by Eq. (26) in Ref. [41]:

$$\frac{\partial}{\partial t}\begin{Bmatrix} \dot{Z} \\ Z \\ \dot{\gamma}_s \\ \gamma_s \\ \dot{\psi} \\ \psi \\ \beta \end{Bmatrix} = \begin{Bmatrix} \left(F_{sZ}+F_{fZ}-F_{cls}\right)/m \\ \dot{Z} \\ \left(M_{sx}+M_{fx}\right)/I+\dot{\psi}^2\gamma_s \\ \dot{\gamma}_s \\ \left[\left(M_{sy}+M_{fy}\right)/I-2\dot{\psi}\dot{\gamma}_s\right]/\gamma_s \\ \dot{\psi} \\ \left\{\beta_{ref}\left[\left(h_{ref}/h\right)\left(\dot{\psi}_r/\omega_{ref}\right)^2\right]-\beta\right\}/\tau \end{Bmatrix} \quad (11)$$

F_{cls} is the net closing force resulting from the circumferential springs, the balance radius, r_b, the hydraulic balance ratio, B (given in Table 1), and the inner and outer pressures as shown in Fig. 1 (see more details in [41]). The initial conditions are:

$$\begin{aligned} &Z(0)=-0.65C_o,\ \gamma_s(0)=\gamma_r, \\ &\dot{Z}(0)=\dot{\gamma}_s(0)=\psi(0)=\dot{\psi}(0)=\beta(0)=0 \end{aligned} \quad (12)$$

The EOMs are integrated in time simultaneously by an efficient multistep ordinary differential equation solver [47]. The same sample seal in [41] is also chosen here with parameters given in Table 1. However, two changes are made: (1) a span of shaft speed cases, ranging within *500-3000 rad/s* in increments of *500 rad/s*, are each simulated, and (2) each simulation is allowed to complete at least 5000 cycles to gather sufficient data sets needed for the spectral analysis.

The numerical simulation produces time series data for the degrees of freedom, Z, γ_s, and ψ, and for the minimum film thickness, h_{min}, as well as other important parameters, e.g., flow Q, and coning, β.

Table 1. Reference case ($\tau = 2$ s, $B=0.75$)

$r_i = 0.0355\ m$	$r_o = r_g = 0.0408\ m$	$\mu = 1.2\cdot10^{-3}\ Pa\ s$	$\gamma_r = 10^{-3}\ rad$
$K_{Zs} = 5\cdot10^5\ N/m$	$D_{Zs} = 300\ N\ s/m$	$F_{spring} = 20\ N$	$m = 1kg$
$\beta_{ref} = 5\cdot10^{-6}\ rad$	$h_{ref} = 0.3\cdot10^{-6}\ m$	$\omega_{ref} = 500\text{-}3000\ rad/s$	$\beta(0) = 0$
$H = 1\ GPa$	$R = 1.7\cdot10^{-6}\ m$	$S_y = 360\ MPa$	$C_o = 10^{-6}\ m$
$E = 24.07\ GPa$	$\sigma = 10^{-7}\ m$	$\psi = 6.167$	$\eta = 4.16\cdot10^{11}$

Because this work is interested in the transients caused by machine noises about steady-state operation, each case is simulated twice: (1) once without any noise, $Z_h=Z_r=0$, and, hence, the results are evidently identical to those in [41], and those are referred to as *"pristine signals,"* and (2) with noises, $Z_h\neq0$, $Z_r\neq0$, the results of which are called *"noisy signals."* The targets herein are the differences between the two solutions, i.e., the *"net signals,"* which are obtained by:

$$NetSignal = NoisySignal - PristineSignal \quad (13)$$

That approach is needed because responses to initial conditions alone do not provide equivalent solutions about steady-state because the system is highly nonlinear. So, in the foregoing, the analysis pertains to the net signal as given in Eq. (13) for all degrees of freedom (DOFs) and parameters of interest.

2.5 Spectral Analysis

The spectral analysis adheres to the procedure outlined in Appendix B in Ref. [42]. The following is a brief summary of that procedure. Suppose the output signal, $x=x(t)$, is the time response to an input noisy excitation, $y=y(t)$. Next, $X=X(f)$ and $Y(f)$ are calculated by (fast) Fourier transforms for both signals. The signals, which are sampled following the Nyquist folding frequency, are analyzed in blocks of time such that there are at least $m=100$ blocks, where $X(f)$ and $Y(f)$ are being averaged over all blocks. That reduces the statistical error by a factor of at least $m^{1/2}=10$. [The Welch method of overlapping windowing is tried as well, producing nearly identical results to regular sequential blocks with no overlapping. That is caused by the very long time-simulations and the long signals produced. Hence, the intended benefit of Welch's method is diminished.] The power spectral densities are:

$$p_x(f)=\frac{2\delta_h}{N}|X(f)|^2;\quad p_y(f)=\frac{2\delta_h}{N}|Y(f)|^2 \quad (14)$$

Where $N=2^{nfft}$ is the number points in each block, $nfft$ is an integer (having a value of 10 or higher), and δ_h is the time interval between sampled points. Therefore, in all results reported herein N is at least 1024 points. The cross spectral density function is:

$$p_{yx}(f)=\frac{2\delta_h}{N}Y^*(f)\cdot X(f) \quad (15)$$

where $Y^*(f)$ is the conjugate of $Y(f)$. All power spectra are also processed by the novel G-Exp filter in [48] to moderate spectral clatter. The transmissibility, is defined as the ratio of output/input:

$$\alpha(f) = \frac{|P_{yx}(f)|}{P_y(f)} \tag{16}$$

The coherence function is also calculated based on p_x, p_y, and p_{yx} (see Ref. [42])), and it is verified to be close to unity (1) to ensure causality between output and input. Of interest here are the transmissibilities of the various parameters, and these are reported below.

3. RESULTS AND DISCUSSION

Out of the range of shaft speeds, Fig. 3 shows the normalized transient responses versus normalized time (i.e., revolutions) for a *1500 rad/s* shaft speed. The select (and most significant) parameters shown are given for the axial degree of freedom, *Z,* nutation γ_s ("gamas"), relative tilt, γ ("gama"), and the minimum film thickness, h_{min}, vs. revolutions. The noisy response is shown in blue, while the pristine response is shown in red. The net signals are taken according to Eq. (13), and then processed spectrally according to section 2.5. Figure 4 shows the power spectrum densities for the said parameters using Eq. (14).

It is obvious that the transients are strong at sub-synchronous frequencies producing rich spectra, with the strongest responses happening near the half frequency whirl (*750 rad/s*), which is expected from the hydrodynamic effect [5,8,29,42]. Noticeable are also strong responses at some super-synchronous speeds which are attributed to face contact and have also been observed experimentally [15,36].

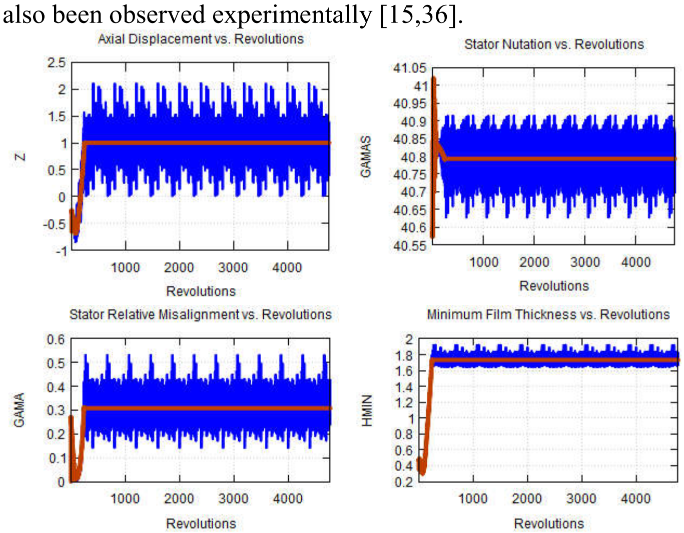

Fig. 3 Transients of output parameters at *1500 rad/s* shaft speed

The process producing Figs. 3 and 4, is repeated for other shaft speeds, ω_{ref}, ranging from *500-3000 rad/s* in increments of *500 rad/s*. Figure 5 shows waterfall plots of the normalized transmissibilities as calculated by Eq. (7) for the said parameters in that shaft speed range (see also Table 1). Figure 5 shows as output the transmissibility sensitivities at various normalized response frequencies, ω/ω_{ref}. While clearly at the synchronous speed, $\omega/\omega_{ref} = 1$ (aka *1X*) peaks are visible, there are rich transmissibility peaks also at sub-synchronous speeds. While the half-frequency whirl (*X/2*) is clearly evident by the strong peak presence at $\omega/\omega_{ref} = 1/2$, peaks are also prevalent at lower and higher sub-synchronous frequencies. Peaks are also visible at super-synchronous frequencies precisely at integer multiples of the shaft speed at *2X, 3X,* etc., being particularly prevalent at shaft speeds larger than *2000 rad/s*. That behavior is a known attribute of seal faces in rubbing contact [15,36].

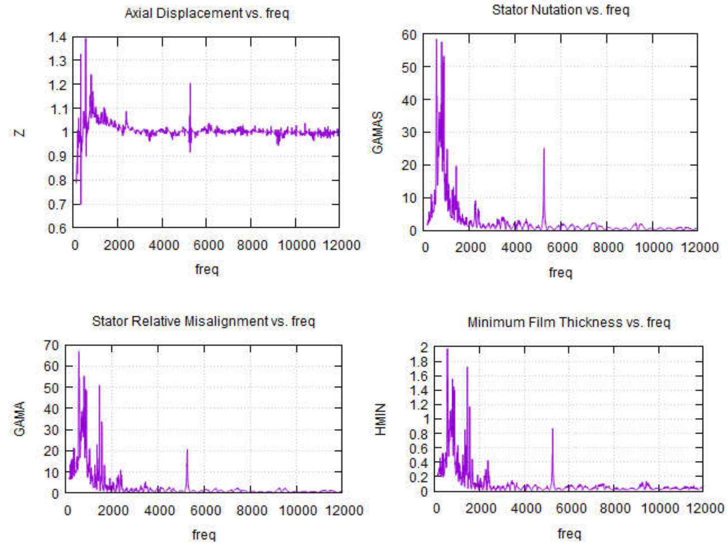

Fig. 4 Power spectrum densities of parameters in Fig. 3

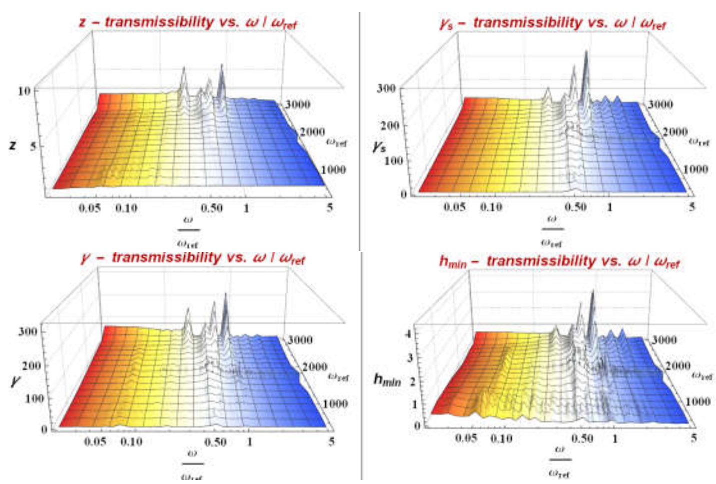

Fig. 5 Waterfall Plots of Parameter Transmissibilities

The discoveries above are reinforced when examining the coning and flow transmissibilities shown in Fig. 6. It is apparent that large flows (leakages) occur correspondingly with large coning transmissibilities that transpire at *0.5X* (at half-frequency whirl), and at *1X* (synchronous whirl), predominantly at above *2000 rad/s*. It is concluded that the investigated seal is safe to operate with predictable low leakage and long-lasting (non-contacting) operation at speed that are lower than *2000 rad/s*. At higher speeds design changes would be needed in some of the seal parameters given in Table 1.

4. CONCLUSION

The objective herein is to provide the theory behind the numerical tools and procedures to investigate the effects that machine vibration imposes upon mechanical face seal transients. The analysis augments existing comprehensive models that have been developed for "pristine" operation. For this highly nonlinear system the analysis focuses upon the resultant response about an equilibrium state. It is clearly evident that at the synchronous speed, *1X*, there are expected strong responses to the rotor misalignment. The magnitudes of the peaks depend upon the magnitudes of the rotor misalignment. The noises, however, result in rich dynamic responses at sub-synchronous and super-synchronous speeds. The *2X, 3X*, etc. components increase their magnitudes with the increase of shaft speeds. These harmonics are attributed to rubbing contact of the seal faces, which are utterly detrimental to seal survivability. The results herein are specific to the sample seal analyzed. Other seal designs are likely to possess dynamic attributes that are similar, along with additional attributes that are specific to a dedicated design or an application.

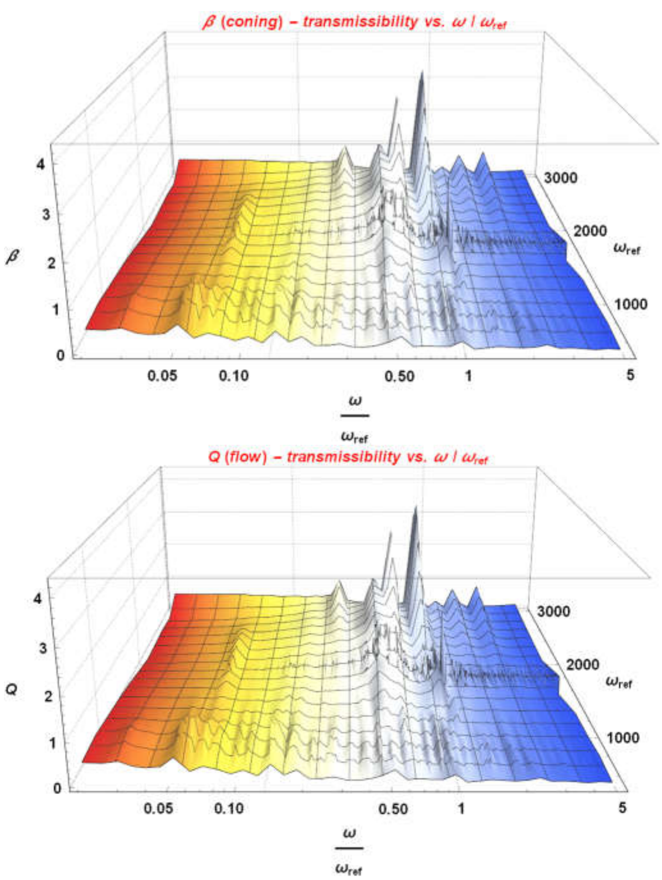

Fig. 6 Waterfall Plots of Coning and Flow Transmissibilities

REFERENCES

[1] Durham, O. M., Williams, H. J., Goldman, J. D., 1990, "Effect of Vibration Failure on Electric-Submersible Pumps Failures," Journal of Petroleum Technology, **42**(2).

[2] Kim, B., Kim, J., Kang, D., Baek, H.-K., and Chung, J., 2021, "Reduction of the Squeal Noise from an Automotive Water Pump," Nonlinear Dyn, **104**(4), pp. 3293–3308.

[3] Stefanko, D. B., and Leishear, R. A., 2005, "Relationship Between Vibrations and Mechanical Seal Failures in Centrifugal Pumps," *Process Industries*, ASMEDC, Orlando, Florida, USA, pp. 5–12.

[4] Green, I., 1983, "Fluid Film Dynamic Coefficients in Mechanical Face Seals," Journal of Lubrication Technology APRIL, **105**, p. 297.

[5] Green, I., and Etsion, I., 1985, "Stability Threshold and Steady-State Response of Noncontacting Coned-Face Seals," ASLE transactions, **28**(4), pp. 449–460.

[6] Green, I., and Etsion, I., 1986, "A Kinematic Model for Mechanical Seals with Antirotation Locks or Positive Drive Devices," Journal of tribology, **108**(1), pp. 42–45.

[7] Green, I., and Etsion, I., 1986, "Nonlinear Dynamic Analysis of Noncontacting Coned-Face Mechanical Seals," ASLE transactions, **29**(3), pp. 383–393.

[8] Green, I., 1987, "The Rotor Dynamic Coefficients of Coned-Face Mechanical Seals with Inward or Outward Flow," Journal of tribology, **109**(1), pp. 129–135.

[9] Green, I., 1990, "Separation Speed of Undamped Metal Bellows Contacting Mechanical Face Seals," Tribology Transactions, **33**(2), pp. 171–178.

[10] Green, I., and Bair, S., 1991, "Dynamic Response to Axial Oscillation and Rotating Seat Runout in Contacting Mechanical Face Seals," Tribology transactions, **34**(2), pp. 169–176.

[11] Wileman, J., and Green, I., 1991, "The Rotordynamic Coefficients of Mechanical Seals Having Two Flexibly Mounted Rotors," Journal of tribology, **113**(4), pp. 795–804.

[12] Green, I., and English, C., 1992, "Analysis of Elastomeric O-Ring Seals in Compression Using the Finite Element Method," Tribology Transactions, **35**(1), pp. 83–88.

[13] Green, I., and English, C., 1994, "Stresses and Deformation of Compressed Elastomeric O-Ring Seals," *14th International Conference on Fluid Sealing*, Mechanical Engineering Publ. London, pp. 83–95.

[14] Lee, A. S., 1993, "The Coupling of Shaft and Mechanical Face Seal Dynamics Using the Complex Extended Transfer Matrix Method," *Rotating Machinery-1992: Proceedings of the Fourth International Symposium on Transport Phenomena and Dynamics of Rotating Machinery (ISROMAC-4)*, Begell House Publishers, p. 262.

[15] Lee, A. S., and Green, I., 1994, "Higher Harmonic Oscillations in a Noncontacting FMR Mechanical Face Seal Test Rig," Journal of vibration and acoustics, **116**(2), pp. 161–167.

[16] Lee, A. S., and Green, I., 1994, "Rotordynamics of a Mechanical Face Seal Riding on a Flexible Shaft," ASME J. Tribol, **116**(2), pp. 345–351.

[17] Lee, A. S., and Green, I., 1992, "Physical Modelling and Data Analysis of the Dynamic Response of a Flexibly Mounted Rotor Mechanical Seal," *Rotordynamics' 92*, Springer, London, pp. 150–157.

[18] Lee, A. S., and Green, I., 1995, "An Experimental Investigation of the Steady-State Response of a Noncontacting Flexibly Mounted Rotor Mechanical Face Seal," Journal of tribology, **117**(1), pp. 153–159.
[19] Wileman, J., and Green, I., 1996, "The Rotor Dynamic Coefficients of Eccentric Mechanical Face Seals," Journal of tribology, **118**(1), pp. 215–224.
[20] Wileman, J., and Green, I., 1997, "Steady-State Analysis of Mechanical Seals with Two Flexibly Mounted Rotors," Journal of tribology, **119**(1), pp. 200–204.
[21] Green, I., 2001, "Real-Time Monitoring and Control of Mechanical Face-Seal Dynamic Behaviour," Sealing Technology, **2001**(96), pp. 6–11.
[22] Zou, M., and Green, I., 1998, "Real-Time Condition Monitoring of Mechanical Face Seal," *Tribology Series*, Elsevier, pp. 423–430.
[23] Wileman, J., and Green, I., 1998, "Stability Analysis of Mechanical Seals with Two Flexibly Mounted Rotors," Journal of tribology, **120**(2), pp. 145–151.
[24] Wileman, J., and Green, I., 1999, "Parametric Investigation of the Steady-State Response of a Mechanical Seal with Two Flexibly Mounted Rotors," Journal of tribology, **121**(1), pp. 69–76.
[25] Zou, M., and Green, I., 1999, "Clearance Control of a Mechanical Face Seal," Tribology Transactions, **42**(3), pp. 535–540.
[26] Zou, M., Dayan, J., and Green, I., 1999, "'Parametric Analysis for Contact Control of a Noncontacting Mechanical Face Seal," Proceedings of Vibration, Noise and Structural Dynamics, **99**, pp. 493–499.
[27] Dayan, J., Zou, M., and Green, I., 2000, "Sensitivity Analysis for the Design and Operation of a Non-Contacting Mechanical Face Seal," Proceedings of the Institution of Mechanical Engineers, Part C: Journal of Mechanical Engineering Science, **214**(9), pp. 1207–1218.
[28] Zou, M., Dayan, J., and Green, I., 2000, "Feasibility of Contact Elimination of a Mechanical Face Seal through Clearance Adjustment," Transactions of the ASME-A-Engineering for Gas Turbines and Power, **122**(3), pp. 478–484.
[29] Green, I., and Barnsby, R. M., 2001, "A Simultaneous Numerical Solution for the Lubrication and Dynamic Stability of Noncontacting Gas Face Seals," Journal of tribology, **123**(2), pp. 388–394.
[30] Miller, B. A., and Green, I., 2001, "Numerical Formulation for the Dynamic Analysis of Spiral-Grooved Gas Face Seals," Journal of Tribology, **123**(2), pp. 395–403.
[31] Green, I., and Barnsby, R. M., 2002, "A Parametric Analysis of the Transient Forced Response of Noncontacting Coned-Face Gas Seals," Journal of tribology, **124**(1), pp. 151–157.
[32] Dayan, J., Zou, M., and Green, I., 2002, "Contact Elimination in Mechanical Face Seals Using Active Control," IEEE Transactions on Control Systems Technology, **10**(3), pp. 344–354.
[33] Miller, B. A., and Green, I., 2002, "Numerical Techniques for Computing Rotordynamic Properties of Mechanical Gas Face Seals," Journal of Tribology, **124**(4), pp. 755–761.
[34] Miller, B. A., and Green, I., 2003, "Semi-Analytical Dynamic Analysis of Spiral-Grooved Mechanical Gas Face Seals," Journal of Tribology, **125**(2), pp. 403–413.
[35] Green, I., 2008, "On the Kinematics and Kinetics of Mechanical Seals, Rotors, and Wobbling Bodies," Mechanism and Machine Theory, **43**(7), pp. 909–917.
[36] Varney, P., and Green, I., 2017, "Impact Phenomena in a Noncontacting Mechanical Face Seal," Journal of Tribology, **139**(2), p. 022201.
[37] Varney, P., and Green, I., 2018, "Dynamic Modeling of an Eccentric Face Seal Including Coupled Rotordynamics, Face Contact, and Inertial Maneuver Loads," Proceedings of the Institution of Mechanical Engineers, Part J: Journal of Engineering Tribology, **232**(6), pp. 732–748.
[38] Green, I., 1989, "Gyroscopic and Support Effects on the Steady-State Response of a Noncontacting Flexibly Mounted Rotor Mechanical Face Seal," Journal of tribology, **111**(2), pp. 200–206.
[39] Jackson, R. L., and Green, I., 2008, "The Thermoelastic Behavior of Thrust Washer Bearings Considering Mixed Lubrication, Asperity Contact, and Thermoviscous Effects," Tribology Transactions, **51**(1), pp. 19–32.
[40] Jackson, R. L., and Green, I., 2006, "The Behavior of Thrust Washer Bearings Considering Mixed Lubrication and Asperity Contact," Tribology Transactions, **49**(2), pp. 233–247.
[41] Green, I., 2002, "A Transient Dynamic Analysis of Mechanical Seals Including Asperity Contact and Face Deformation," Tribology transactions, **45**(3), pp. 284–293.
[42] Green, I., and Etsion, I., 1986, "Pressure and Squeeze Effects on the Dynamic Characteristics of Elastomer O-Rings under Small Reciprocating Motion," Journal of tribology, **108**(3), pp. 439–444.
[43] Chang, W. R., Etsion, I., and Bogy, D. B., 1987, "An Elastic-Plastic Model for the Contact of Rough Surfaces," Journal of Tribology, **109**(2), p. 257.
[44] Jackson, R. L., and Green, I., 2005, "A Finite Element Study of Elasto-Plastic Hemispherical Contact against a Rigid Flat," Journal of tribology, **127**(2), pp. 343–354.
[45] Jackson, R. L., and Green, I., 2006, "A Statistical Model of Elasto-Plastic Asperity Contact between Rough Surfaces," Tribology International, **39**(9), pp. 906–914.
[46] Green, I., 2019, "Exact Spectral Moments and Differentiability of the Weierstrass-Mandelbrot Fractal Function," Journal of Tribology, pp. 1–18.
[47] Shampine, L. F., 1994, *Numerical Solution of Ordinary Differential Equations*, Chapman and Hall/CRC, New York.
[48] Green, I., 2020, "Metrology and Numerical Characterization of Random Rough Surfaces—Data Reduction via an Effective Filtering Solution," Proceedings of the Institution of Mechanical Engineers, Part J: Journal of Engineering Tribology, **234**(9), pp. 1452–1469.

